Materials Science & Engineering A 842 (2022) 143086

Contents lists available at ScienceDirect

Materials Science & Engineering A

journal homepage: www.elsevier.com/locate/msea

Comparison of the creep-fatigue cyclic life saturation effect for three different superalloys

Biao Ding [a], Weili Ren [a,*], Yunbo Zhong [a,**], Xiaotan Yuan [a], Tianxiang Zheng [a], Zhe Shen [a], Yifeng Guo [a,***], Qiang Li [a], Chunmei Liu [a], Jianchao Peng [b], Josip Brnic [c], Yanfei Gao [d], Peter K. Liaw [d]

[a] State Key Laboratory of Advanced Special Steel, College of Materials Science and Engineering, Shanghai University, Shanghai, China
[b] Laboratory for Microstructures, Shanghai University, Shanghai, China
[c] University of Rijeka, Faculty of Engineering, Vukovarska 58, 51000, Rijeka, Croatia
[d] Department of Materials Science and Engineering, The University of Tennessee, Knoxville, USA

ARTICLE INFO

Keywords:
Superalloy
Creep-fatigue
Cyclic life saturation
Mechanical response
Damage mechanism

ABSTRACT

This investigation reports the results of the strain-controlled creep-fatigue behavior of precipitation-strengthened directionally-solidified Nickel-based superalloy DZ445. The results refer to the processes performed at 850 °C in the total strain range of 1.0% with 0, 3, 10, and 30 min tensile-dwell time. It was found that, compared to cyclic life that decreases rapidly after the initial application of dwell time, the reduced cyclic life slows down gradually when the dwell time exceed 30 min (i.e., the "generalized saturation effect"). As the publicly reported creep-fatigue results of the solid-solution-strengthened superalloy Haynes 230 and Alloy 617 under the same loading conditions, the cyclic life continues to decrease even 30 min dwell time is reached, which is hard to reach the case of N_f saturation. The reasons to reach the cyclic life (N_f) saturation are systematically elaborated from two aspects, namely, mechanical response (maximum stress, plastic strain, hysteresis loop, stress relaxation, etc.), and damage mechanism (cracks, voids, dislocation structures, etc.). This research provides theoretical guidelines for achieving the safety design of the superalloy components in the creep-fatigue deformation.

1. Introduction

The fatigue properties of the structural materials are usually considered in most construction projects [1]. Particular attention should be paid to predicting and preventing possible component failures due to fatigue, especially when considering fatigue behavior with dwell times [2]. Superalloys are widely used in aviation/gas engines and hot-end components of nuclear power due to their excellent properties regarding strength, plasticity, fracture toughness, fatigue- and corrosion-resistance at high temperatures [2,3]. Due to the frequent start-up, shut-down, and stress fluctuation during the operation time of engine/nuclear power plant, these superalloys usually suffer from creep-fatigue interactive damage [4,5]. A complete creep-fatigue database is very critical for the safety design of these components [6]. Therefore, the creep-fatigue behavior of superalloy has become a research hotspot in recent years [7–10].

Many previous studies have shown that the creep-fatigue properties of materials depend on temperature [11], strain range [12], waveform [13], and dwell time [14]. With the dwell time of tensile (or compressive) strain (or stress), the creep-fatigue life (N_f) of some alloys shows a continuous decreasing trend [15,16]. However, under certain conditions, the reduction of N_f for some alloys gradually slows down or even hardly continues to decrease with the increasing dwell time [17–22]. This phenomenon was referred to as the generalized "saturation effect" of cycle life. This "saturation phenomenon" was first observed in the creep-fatigue deformation of austenitic stainless steel [17]. Publicly reported data show that under appropriate loading conditions, the mentioned phenomenon will exist in the creep-fatigue behavior of 304 L stainless steel [18], 316 stainless steel [19], titanium alloys [23,24], as well as at different types of superalloys [25–27]. For example, in the

* Corresponding author.
** Corresponding author.
*** Corresponding author.
E-mail addresses: wlren@staff.shu.edu.cn (W. Ren), yunboz@staff.shu.edu.cn (Y. Zhong), yfguo@shu.edu.cn (Y. Guo).

https://doi.org/10.1016/j.msea.2022.143086
Received 23 November 2021; Received in revised form 27 March 2022; Accepted 1 April 2022
Available online 10 April 2022

creep-fatigue deformation of precipitation-strengthened directionally--solidified superalloy (DS) DZ125 [14] and the solid-solution-strengthened superalloy GH4169, the N_f keeps almost unchanged when 2 and 5 min dwell time is imposed at the maximum strain [12]. For the solid-solution-strengthened Alloy-800H at 850 °C and the total strain range of 0.3%, 0.6%, 1.0% and 1.5%, respectively, the N_f saturation effect occurs in all conditions when the dwell time reaches 30 min [21]. The creep-fatigue experiments on Alloy 617 were conducted at 850 °C and 950 °C with the total strain range of 0.3% and 1.0%, respectively [20,25]. The results show that there is no life "saturation phenomenon" at 850 °C when the dwell time increased to 30 min. The author believed that this was because the stress at the dwell-period would continue to relax after 30 min dwell time [25]. However, the rapid saturation phenomenon of N_f at 950 °C is attributed to the stress at the dwell-period reaching the relaxation limit in a short time [26].

In the above-mentioned literature, it is stated, in fact, that when a certain dwell-time is reached, the life of creep - fatigue will become saturated under certain load conditions. Most previous researches have only described the "saturation phenomenon" of cyclical life with long dwell time. However, there is no systematic explanation regarding this interesting and important phenomenon. The creep-fatigue experiments for the precipitation-strengthened DZ445 DS superalloy at 850 °C and a total strain range of 1.0% were investigated in detail here (The reason for choosing strain-control mode is that in many structural components, especially for the blade root blades, the strain-control condition often occurred due to the elastic constraints of the surrounding materials). Comparing the creep-fatigue data for the DZ445 superalloy with those of the Haynes 230 superalloy and the solid solution reinforced Alloy 617 under the same load conditions [27], the mechanism of these "the occurrence condition of N_f saturation" in terms of mechanical response and damage mechanism was clarified. The idea of evaluating the creep-fatigue performance of superalloys with cyclic life and the fracture time is also proposed. This investigation will provide theoretical guidance for the creep-fatigue safety design of superalloy components and the establishment of related constitutive equations.

2. Experiment

2.1. Materials

The precipitation-strengthened DZ445 superalloy, considered in this investigation, is a directionally-solidified columnar nickel-based superalloy with outstanding high-temperature strength, oxidation resistance, high-temperature creep performances, and fatigue properties [28,29]. Some detailed metallographic structure after heat treatment of DZ445 superalloy (the heat treatment regime: 1210 °C ± 10 °C/2 h/AC + 1080 °C ± 10 °C/3 h/AC+ 850 °C ± 10 °C/24 h/AC, AC: air cooling) is shown in Fig. 1(a). The compositional segregation between the dendrites and the interdendrites is slowed down. Fig. 1(b) shows the typical cubic γ′ precipitates of DZ445 superalloy after heat treatment. Other detailed microstructure of DZ445 superalloy before and after heat treatment were considered in our previous investigation [30]. Solid-solution-strengthened superalloy - Alloy 617 is a nickel-chromium-cobalt-molybdenum alloy with excellent mechanical properties at high temperatures [26]. The microstructure of Alloy 617 after solution aging is shown in Fig. 1(c). The grain size was about 150 μm, and the carbides were distributed in the matrix. Haynes 230 is a Ni–Cr-based solid-solution-strengthened wrought superalloy, which contains a large amount of tungsten, a small amount of aluminum and titanium. It has outstanding oxidation resistance, stamping, and welding performance [31]. The microstructure of Haynes 230 with solid-solution-aged state is shown in Fig. 1(d). M_6C type carbides were dispersed in the matrix, and the twin boundaries could also be observed. The composition of three different strengthening types of superalloys and their mechanical properties at 850 °C are listed in Tables 1 and 2, respectively. The strength of DZ445 superalloy is much higher than that of the other two superalloys at 850 °C.

2.2. Low-cycle fatigue and creep-fatigue tests

The diameter and gauge length of the sample in the creep-fatigue test

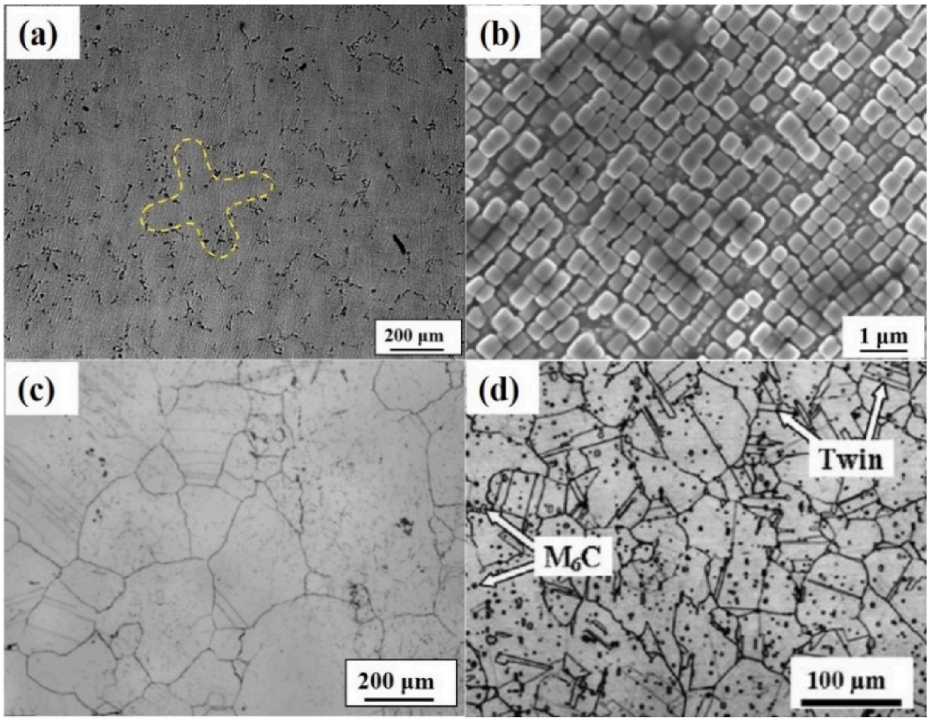

Fig. 1. (a) Optical structure of DZ445 superalloy after heat treatment (the yellow dotted line is the dendritic structure); (b) γ′ precipitates; (c) optical micrograph of the solution-annealed Alloy 617 [26]; and (d) Haynes 230 [31]. (For interpretation of the references to colour in this figure legend, the reader is referred to the Web version of this article.)

Table 1
Composition in wt. % of DZ445 superalloy, Haynes 230 [32], and Alloy 617 [33].

Materials	Ni	C	Cr	Co	Mo	Al	Ta	Ti	Mo	Mn	Fe	W
DZ445	Bal	0.07	13.1	9.99	1.75	4.07	4.8	2.38	1.75	/	/	4.53
Haynes 230	Bal	0.1	22.4	0.07	1.21	0.32	/	/	1.21	0.5	0.64	14.4
Alloy 617	Bal	0.05	22.2	11.6	8.6	1.6	/	0.4	/	0.1	1.6	/

Table 2
Elastic modulus and yield strength of DZ445 superalloy, Haynes 230 [32], and Alloy 617 [33] at 850 °C.

Parameter/Materials	DZ445	Haynes 230	Alloy 617
Yield strength (MPa)	670.0	270.0	260.0
Elasticity modulus (GPa)	102.5	160.5	153.0

were Φ 8.5 mm and 26 mm, respectively. Prior to the creep-fatigue experiments, the surface of sample's gauge length and transition arc was finely polished with abrasive paper. Then, the sample was treated with the diamond polishing paste to remove possible surface imperfections of the sample. The surface roughness (Ra) after polishing is about 0.2 μm. All the strain-controlled creep-fatigue experiments were performed on RPL series electronic creep-fatigue testing machines. The experiment was controlled by a triangular wave in the case of no dwell time. The dwell times of 3, 10, and 30 min were introduced at the maximum tensile strain 0.5% to form a trapezoidal wave, respectively. The strain ratio R ($R = \varepsilon_{min}/\varepsilon_{max} = -0.5\%/0.5\%$) was −1 (which is consistent with the creep-fatigue load conditions of Haynes 230 and Alloy 617 as stated in the literature [27]). Three K-type thermocouples were used to monitor the temperature at top, middle, and bottom parts of the sample surface. After heating to the target temperature of 850 °C, the temperature was kept for 10 min to ensure the temperature uniformity of the whole sample. Throughout the experiment, the temperature fluctuation along the gauge length would not exceed ±2 °C. The rail-type high-temperature extensometer was used to control the presupposed total strain. Each experiment was performed until the sample was completely fractured. The fracture was regarded as the effective experiment when the fracture is within the gage section. The creep-fatigue life was defined as the number of cycles (N_f) when the sample was completely broken. Each experiment was repeated 2–3 times to ensure data repeatability and reliability.

2.3. Characterization

A scanning electron microscope (SEM) was used to observe the fracture surface. The etchant composed of 20 ml HCl +5 g $CuSO_4$ + 25 ml H_2O. More than 10 figures within 1 mm below the fracture are taken to observe the cracks and the voids. Thin slices about 200 μm thickness were cut 2–3 mm below the fracture, along the direction perpendicular to the stress axis, to prepare the transmission electron microscopy (TEM) samples. They were then punched into small discs with a diameter of 3 mm. Finally, they were prepared with #800, #1500, and #3000 abrasive paper to the thickness of about 50 μm. Then, an electrolyte composed of 10% perchloric acid +90% ethanol was used for twin jet polishing at −30 °C and 40 V. The dislocation structures were observed in JEOL JEM-2010 TEM under 200 kV acceleration voltage using bright and dark fields and with two-beam conditions.

3. Results

3.1. Fatigue life

Previous investigations [25,34] described the creep-fatigue behavior of solid-solution-strengthened superalloys Haynes 230 and Alloy 617 at 850 °C with a total strain range of 1.0%. In order to investigate the creep-fatigue life for different strengthening types of superalloys with dwell time in detail, the creep-fatigue tests were conducted on the precipitation-strengthened superalloy DZ445 under the same loading conditions. The specific experimental parameters and results are shown in Fig. 2 (a) and Table 3. To show the change trend of the fatigue life for each superalloy clearly, the creep-fatigue data of Haynes 230 and Alloy 617 are separately shown in Fig. 2 (b). The fatigue life is significantly reduced after the initial dwell time is applied for DZ445 superalloy. Compared to the case about the initial application of 3 min dwell time, the reduction in fatigue life is gradually decreased when the dwell time exceeds 10 min. Moreover, our creep-fatigue results at 900 °C with a total strain of 1.6% also show that with the application of a longer dwell time (more than 16 min), the cyclic life not only does not continue to decline, but even to raise again. While for Haynes 230 and Alloy 617, the fatigue life seems to be decreased continuously with the application of dwell time. The statistical results of the absolute and relative reduction of the cyclic life with dwell time for these three superalloys are also shown in Table 4. Compared with the life in pure fatigue, the absolute reduction of the cyclic life for DZ445 superalloy is 2578, 1802, and 112 cycles with 3, 10, and 30 min dwell time, respectively. The relative change for them is 0.4472, 0.5654, and 0.0809, respectively. These statistics show that the fatigue life is almost similar when the dwell time exceed 10 min. That is, the generalized N_f "saturation phenomenon" is more prone to occur. For Alloy 617, after 3, 10, and 30 min of dwell time are applied, the absolute reduction of fatigue life are 111, 204, and 92 cycles, respectively; the relative variation are 0.1470, 0.3168, and 0.2091, respectively. Even when the dwell time is as long as 240 min, the fatigue life of Alloy 617 also shows a decreasing trend [25]. It indicates that the N_f saturation effect is more difficult to occur. The change trend of N_f for Haynes 230 with dwell time is also similar to that of Alloy 617 [Fig. 2 (b) and Table 3]. The creep-fatigue N_f saturation effect occurs in which cases. It is related to the material category, the mechanical response, and the damage mechanism [35]. The behavior of creep-fatigue N_f saturation related to these three superalloys would be analyzed in detail below.

3.2. Mechanical response

3.2.1. Stress response

Fig. 3 (a) shows the maximum tensile-stress of DZ445 superalloy at 850 °C and a total strain of 1.0% with different dwell times. The maximum stress is almost flat during the entire deformation process until the stress drops quickly in the case of without dwell time, corresponding to the macroscopic crack propagation at the end of deformation. After the dwell time is applied, the maximum tensile stress in the initial cycles is similar. Then, it drops rapidly to reach an approximate steady state. Another kind of precipitation-strengthened single-crystal superalloy CMSX-8, also shows a similar trend in stress response [36]. As the dwell time increases from 10 to 30 min, the maximum tensile stress in the stable deformation stage is almost similar. The N_f saturation effect could be well explained by the similar maximum stress response. From Fig. 3 (b), (c) and (d), the maximum tensile stress of Haynes 230 and Alloy 617, which are mainly strengthened by solid solution, continue to decrease throughout the deformation stage. Reducing peak stress is directly related to the worsening damage. In other creep-fatigue studies of Alloy 617 [37] and martensitic steel [38,39], the maximum stress response also shows a trend of continuous softening. This phenomenon is associated with the process of thermal activation in connection with dislocation recovery. The strain-dwell period provides more time for

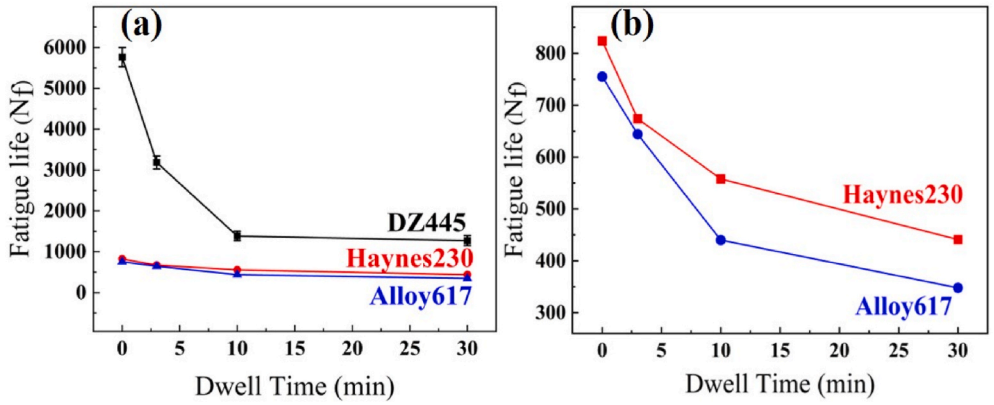

Fig. 2. Relationship between tensile-dwell time and creep-fatigue life of DZ445 superalloy, Alloy 617 [27], and Haynes 230 [27] at a total strain range of 1.0% and 850 °C (a). Fig. (b) is the partial enlarged view of image (a).

Table 3
Creep-fatigue test parameters and results of DZ445 superalloy, Alloy 617 [27], and Haynes 230 [27] at a total strain range of 1.0% and 850 °C.

Materials	The length of gage section (mm)	Dwell Time (min)	Fatigue life (N_f)	Fracture time (hr)
DZ445	25	0	5765	6.39
DZ445	25	3	3187	166.89
DZ445	25	10	1385	230.83
DZ445	25	30	1273	640.21
Haynes 230	6	0	824	18.31
Haynes 230	6	3	674	48.68
Haynes 230	6	10	558	105.40
Haynes 230	6	30	441	230.30
Alloy 617	12	0	755	4.19
Alloy 617	12	3	644	35.77
Alloy 617	12	10	440	75.77
Alloy 617	12	30	348	175.93

Table 4
Variation of N_f reduction during different dwell time periods for Alloy 617 [27], Haynes 230 [27], DZ445 superalloy. ("A" represents the absolute variation and "R" represents the relative variation. The lower right corner marks represent different dwell-periods, the unit is minute.)

Materials/Variation	$A_{0\text{-}3}$	$R_{0\text{-}3}$	$A_{3\text{-}10}$	$R_{3\text{-}10}$	$A_{10\text{-}30}$	$R_{10\text{-}30}$
DZ445	2578	0.4472	1802	0.5654	112	0.0809
Haynes 230	150	0.1820	116	0.1721	117	0.2097
Alloy 617	111	0.1470	204	0.3168	92	0.2091

dislocation rearrangement and annihilation [40]. The essential reason for the change of tensile-stress with cyclic life will be explained in detail in the section of dislocation analysis.

The turning point between the initial rapid softening and the subsequent period of steady stress period is called as characteristic cycle [as shown in Fig. 3(a)]. Table 5 quantifies the cyclic softening/hardening parameters in different deformation stages for the three superalloys in detail. When the dwell time exceeds 10 min, the saturation degree of the maximum tensile stress for DZ445 superalloy corresponds to the no longer continuous decrease of cyclic life. The cyclic softening degree of the maximum tensile stress for Haynes 230 and Alloy 617 increases continually with dwell time, corresponding to the gradual increases of damage. Therefore, the fatigue life decreases continuously. The plastic strain is also an important parameter to control material damage [41]. The influence of dwell time on the plastic strain for these three superalloys will be analyzed in detail as follow.

3.2.2. *Plastic strain*

The range between the two intersection points of the hysteresis loop and the abscissa is defined as the plastic strain [42]. The statistical results of plastic strain (ε_P), elastic strain (ε_E), and their ratio ($\varepsilon_P/\ \varepsilon_E$) for these three superalloys are shown in Table 6. The plastic strain range of DZ445 superalloy with the same total dwell time is much smaller than the value of the solid solution-strengthened superalloy Haynes 230 and Alloy 617. It also indicates to the longer fatigue life of DZ445 superalloy. Regardless of what kind of superalloy, the initial application of the dwell time significantly increases the plastic strain, resulting in a decrease of fatigue life. As the dwell time increases from 3 to 30 min, the plastic strain range of Haynes 230 and Alloy 617 continues to increase, which corresponds to the continuous decrease in fatigue life. Although the plastic strain range of the DZ445 superalloy is further increased when the dwell time exceeds 10 min, the increase in the plastic strain range is greatly reduced compared to the case with the initial application of 3 min. The downward trend of fatigue life for DZ445 superalloy is gradually reduced accordingly. The introduction of plastic strain mainly occurs in the tensile-strain dwell period, which also changes the shape and area of the hysteresis loop.

3.2.3. *Hysteresis loop*

There are some limitations to evaluate material damage by using the parameter of stress or strain separately. However, the stress and strain parameters could be combined in the hysteresis loop. Fig. 4 shows the hysteresis loops of DZ445, Haynes 230 [27], and Alloy 617 [27] in the half-life cycle at a total strain of 1.0% and 850 °C with different dwell times. The area of the hysteresis loop is usually used as the measure of resistance to inelastic-strain deformation (inelastic strain energy, ΔU_{in}) [12]. The expression is,

$$\Delta U_{in} = \alpha \times \sigma_T \times \Delta\varepsilon_{in} \tag{1}$$

where α, σ_T, and $\Delta\varepsilon_{in}$ are the shape factor, the maximum tensile-stress, and the inelastic-strain, respectively. Halford once proposed the expression of the shape factor as [43],

$$\alpha = \frac{1}{1+n'} \tag{2}$$

where n' is the cyclic strain hardening index, which could be determined from the cyclic stress-strain curve obtained by the low-cycle-fatigue experiments. According to the relevant data in previous work [27,44], the n' of DZ445, Haynes 230, and Alloy 617 at 850 °C are calculated as 0.2688, 0.0469, and 0.0309, respectively.

The estimated value of ΔU_{in} based on the data about the above maximum tensile stress, plastic strain, cyclic strain hardening index, and Eq. (1) are listed in Table 7. As shown in Fig. 4 (a), compared with the hysteresis loop in pure fatigue, the enclosed area is greatly increased

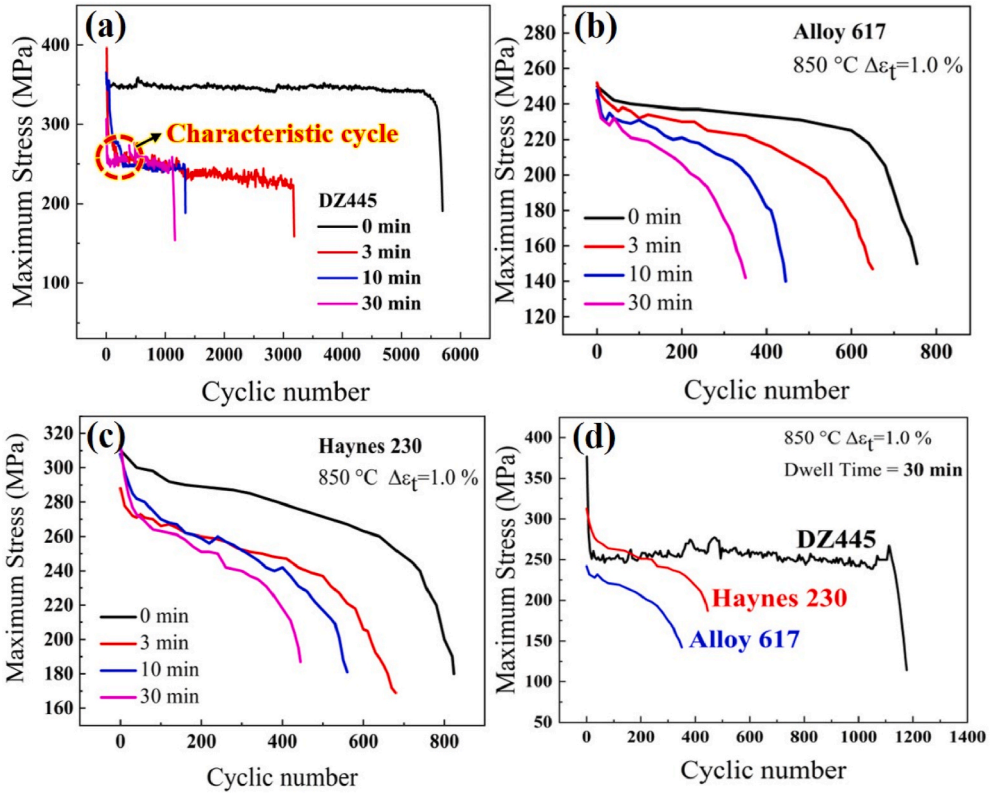

Fig. 3. The maximum tensile stress vs. the cyclic number with different dwell time for DZ445 superalloy at a total strain of 1.0% and temperature of 850 °C (a); for Alloy 617 [27], Haynes 230 [27], and DZ445 superalloy with dwell time of (b) 3 min; (c) 10 min; (d) 30 min.

Table 5
Cyclic softening/hardening parameters of DZ445 superalloy, Haynes 230 [27], and Alloy 617 [27] at different stages in creep-fatigue deformation. The D_T, N_{init}, σ_{first}, σ_{steady}, σ_{half}, SAF_{init}, and SAF_{sub} represent the dwell time, the number of cycles at the characteristic cycle, the maximum stress at the first cycle, the characteristic cycle, the half-life cycle, the amplitude factor of the initial rapid softening stage and the subsequent slight softening/hardening stage, respectively.

Materials	D_T(min)	N_{init}	σ_{first} (MPa)	σ_{steady} (MPa)	σ_{half} (MPa)	SAF_{init}	SAF_{sub}
DZ445	0	12	385.96	369.51	367.15	0.0426	0.0063
DZ445	3	181	384.51	260.36	215.24	0.3229	0.1733
DZ445	10	175	382.61	262.29	247.16	0.3141	0.0573
DZ445	30	25	376.78	250.89	253.09	0.3341	−0.0088
Haynes 230	3	10	288.00	278.00	256.75	0.0347	0.0764
Haynes 230	10	30	308.00	285.00	254.53	0.0747	0.1069
Haynes 230	30	30	313.00	277.00	251.02	0.1150	0.0938
Alloy 617	3	10	252.00	245.00	224.87	0.0278	0.0822
Alloy 617	10	10	248.00	235.00	221.52	0.0524	0.0573
Alloy 617	30	10	242.00	225.00	210.20	0.0703	0.0658

Table 6
Plastic strain range (ε_P), elastic strain range (ε_E), and the ratio of them ($\varepsilon_P/\varepsilon_E$) at half-life cycle with DZ445 superalloy, Haynes 230 [27], and Alloy 617 [27] at a total strain range of 1.0% and temperature of 850 °C.

Materials	Dwell time (min)	ε_P (%)	ε_E (%)	$\varepsilon_P/\varepsilon_E$
DZ445	0	0.0534	0.9466	0.0564
DZ445	3	0.1401	0.8599	0.1629
DZ445	10	0.1771	0.8229	0.2152
DZ445	30	0.1817	0.8183	0.2220
Haynes 230	3	0.8021	0.1979	4.0531
Haynes 230	10	0.8224	0.1776	4.6306
Haynes 230	30	0.8304	0.1696	4.8962
Alloy 617	3	0.8233	0.1767	4.6593
Alloy 617	10	0.8348	0.1652	5.0533
Alloy 617	30	0.8394	0.1606	5.2267

with dwell time. The similar shape and enclosed area of the hysteresis loop after the application of 10 and 30 min dwell time correspond to the "generalized saturation" of cyclic life. Comparing Fig. 4 (b), (c) and (d), under the same total dwell time, the hysteresis loop area of the solid-solution-strengthened Haynes 230 and Alloy 617 is much larger than that of the DZ445 superalloy. It shows that the ability of solid-solution-strengthened superalloys to resist deformation is weaker than that of DZ445. The plastic strain energy reaches the critical value of fracture quickly, which corresponds to a lower fatigue life of Haynes 230 and Alloy 617 alloys. But for the two solid-solution-strengthened superalloys, the shape and area of the hysteresis loop with 3–30 min of dwell time are also relatively similar. It seems that the saturation effect of cyclic life should be appeared theoretically. However, in fact, the fatigue life continues to decrease with the increase of dwell time. This result may be caused by statistical errors because the similar ΔU_{in} after the dwell time is applied. It also indicates that the "saturation" of fatigue life is not only caused by mechanical response, but also related to the

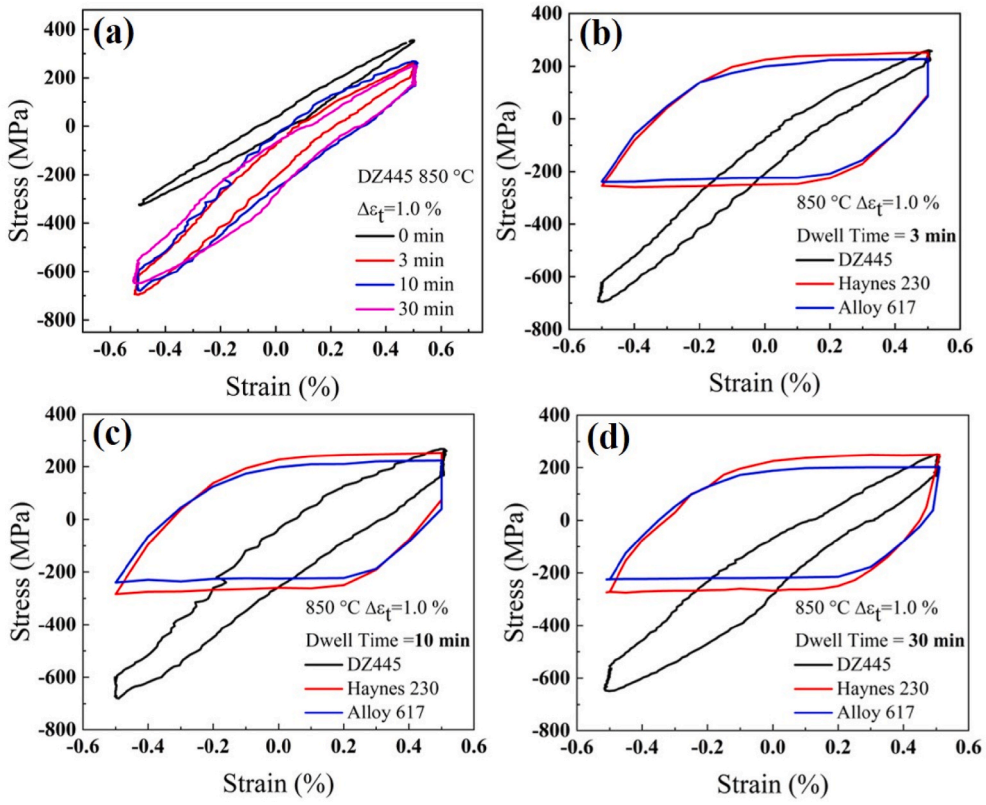

Fig. 4. Hysteresis loop of DZ445 superalloy under different dwell time in half-life cycle at a total strain range of 1.0% with temperature of 850 °C (a). Hysteretic loop of DZ445 superalloy, Haynes 230 [27], and Alloy 617 [27] with different dwell time (b) 3 min; (c) 10 min; (d) 30 min.

Table 7
Inelastic strain energy (ΔU_{in}) at half-life cycle with DZ445 superalloy, Haynes 230 [27], and Alloy 617 [27] at a total strain range of 1.0% with temperature of 850 °C.

Materials	DZ445				Haynes 230				Alloy 617			
Dwell time (min)	0	3	10	30	0	3	10	30	0	3	10	30
ΔU_{in} **(MJ/m^3)**	0.1316	0.2433	0.3248	0.3041	1.8492	1.9671	1.9995	1.9910	1.7458	1.7958	1.7939	1.7116

deformation mechanism.

3.2.4. Stress relaxation

Fig. 5 (a) shows the relationship between the stress during the tensile-dwell period with dwell time in the half-life cycle at a total strain of 1.0% and 850 °C for DZ445 superalloy. The stress relaxation curve shows the following three stages: rapid softening, transition period, and final steady stage region, whose trend is similar to the pure stress relaxation behavior of different types of superalloys [45,46]. The amount of stress relaxation is the smallest with dwell time of 3-min. The corresponding fatigue life is also the largest. With the dwell time of 10 and 30 min, the amount of stress relaxation increases and they are closer to each other. The difference between their fatigue life is also small. Fig. 5 (b), (c) and (d) show the relationship between the relaxed stress with dwell time of Alloy 617 [27], Haynes 230 [27], and the DZ445 superalloy, respectively. Under the same total dwell time, the amount of stress relaxation of Haynes 230 and Alloy 617 is much greater than that of DZ445 superalloy, which corresponds to the lower fatigue life of Haynes 230 and Alloy 617 alloy. The biggest difference is that regardless of the total dwell time, stress during the dwell period of Alloy 617 and Haynes 230 continue to relax and doesn't reach the saturated state. It reflects in the absence of creep-fatigue life "saturation" for these two superalloys at 850 °C until dwell time of 30 min. While for Alloy 617 at 950 °C, the stress relaxation reaches a saturated state quickly in the creep-fatigue at the same strain range [47]. The "saturation effect" of cycle life would be present. Essentially, the process of stress relaxation is a process of Gibbs free energy reduction [48]. The stress relaxation reaches a steady state when the Gibbs free energy reaches its minimum. It also agrees with the subsequent explanation that the cyclic life only appear in a saturated state when the dislocation generation and annihilation reach dynamic equilibrium.

In order to show the effects of different strengthening types and total dwell time on stress relaxation more clearly, the initial value (σ_{init}), the ending value (σ_{end}), the stress relaxation amount ($\Delta\sigma$), and the $\Delta\sigma/\ \sigma_{init}$ in Fig. 5 are shown in Table 8. Since the higher initial stress value results in the greater amount of stress relaxation within the same relaxation time [47]. Therefore, considering the amount of stress relaxation simply may be biased, the $\Delta\sigma/\ \sigma_{init}$ should be considered comprehensively. The $\Delta\sigma/\ \sigma_{init}$ of DZ445 superalloy under the conditions of 3, 10, and 30 min total dwell time are 0.1632, 0.3781, and 0.3714, respectively. The stress relaxation gradually reaches a saturated state with dwell time. While the $\Delta\sigma/\ \sigma_{init}$ of the solid-solution-strengthened superalloy Haynes 230 and Alloy 617 increase continuously with dwell time, which indicates that the relaxation has not reached the steady state. The stress relaxation behavior corresponds to the continuous decline in the creep-fatigue life of these two kinds of solid-solution-strengthened superalloys.

The detailed discussions of "comparison of the creep-fatigue cyclic life saturation effect for three different superalloys" is given above from the perspective of mechanical response. The cyclic loading will lead to the appearance of surface cracks, and the stress relaxation caused by the

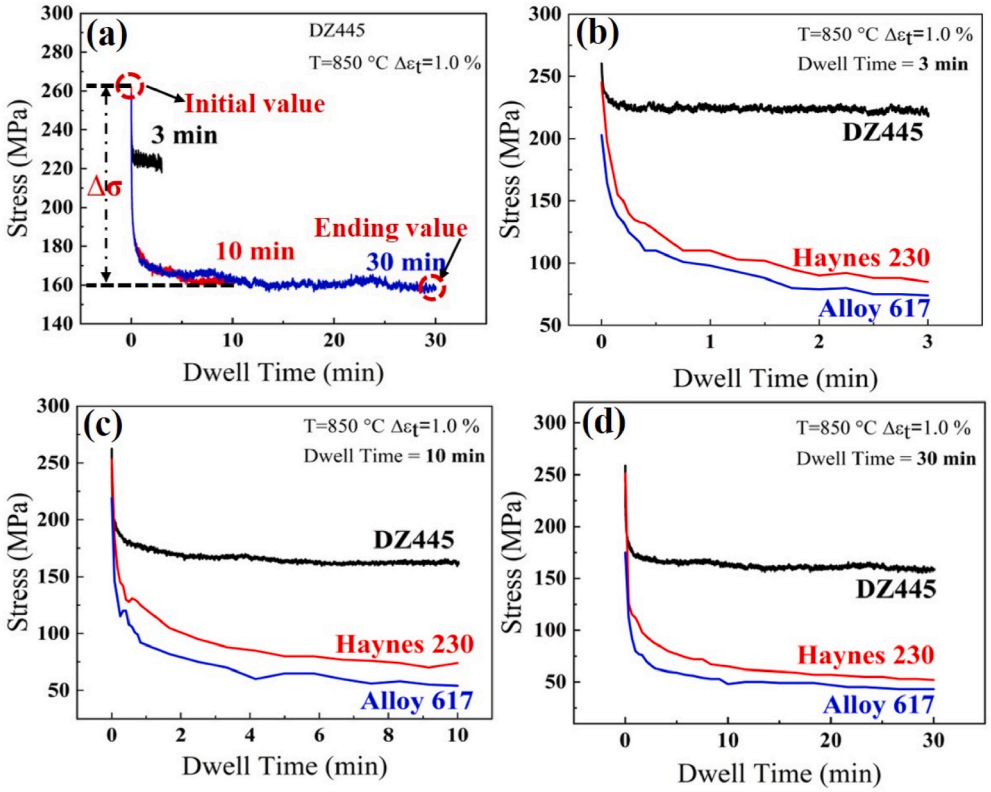

Fig. 5. Relationship between the stress in the dwell-period and the dwell time at the half-life cycle with different total dwell time for DZ445 superalloy (a); Haynes 230 [27], and Alloy 617 [27] (b) 3 min; (c) 10 min; (d) 30 min at a total strain of 1.0% and temperature of 850 °C.

Table 8
Stress relaxation parameters at half-life cycle of DZ445 superalloy, Haynes 230 [27], and Alloy 617 [27] under a total strain of 1.0% and temperature of 850 °C with different dwell time. N_{init}, σ_{end}, and $\Delta\sigma$ represent the initial value, the ending value of stress, and the amount of stress relaxation during the dwell period.

Material	Dwell time (min)	σ_{init} (MPa)	σ_{end} (MPa)	$\Delta\sigma$ (MPa)	$\Delta\sigma/\sigma_{init}$
DZ445	3	260.36	217.88	42.48	0.1632
DZ445	10	262.56	163.27	99.39	0.3785
DZ445	30	250.89	157.70	93.19	0.3714
Haynes 230	3	256.75	85.00	171.75	0.6689
Haynes 230	10	254.53	70.00	184.53	0.7249
Haynes 230	30	251.02	52.00	199.02	0.7929
Alloy 617	3	224.87	70.00	154.87	0.6887
Alloy 617	10	221.52	50.00	171.52	0.7743
Alloy 617	30	210.20	43.00	167.20	0.7954

dwell period result in the growth of plastic voids [49]. Thus, the inherent relationship between the damage mechanism and N_f "saturation effect" for different kinds of superalloys will be analyzed as follow.

3.3. Damage mechanism

3.3.1. Fractography

Fig. 6 shows a partially enlarged view of the creep-fatigue fracture for the precipitation-strengthened DZ445 superalloy at a total strain of 1.0% and 850 °C with different dwell times. The upper right insert in Fig. 6 represents a complete view of the fracture. The area bounded by the yellow dashed line is the crack initiation area. Fig. 6(a) shows that the cracks formed under pure fatigue originate from the sample surface. It is similar to the characteristics for other types of superalloys under pure fatigue load [50,51]. A fracture with 3 min dwell-time [Fig. 6(b)] shows the propagation of fatigue cracks and obvious intergranular cracks and voids (the grain boundaries of DZ445 superalloy are parallel to the direction of loading. The "intergranular" fracture mainly refers to the γ/γ' phase interface or the dendritic stem/intermediate in the directionally-solidified columnar/single-crystal superalloy). The interaction of these cracks and voids accelerates the propagation of cracks and reduces the fatigue life [52,53]. As shown in Fig. 6(c) and (d), the ratio of voids and plastic tearing cracks under 10- and 30-min dwell time is further increased. In contrast to the brittle fracture, the characteristics of mixed creep/plastic fracture indicate a delay in the crack propagation, making the gradual slower decline of cyclic life [54].

From the previous literatures, no detailed fracture for the creep-fatigue of solid-solution-strengthened Haynes 230 and Alloy 617 under the same loading conditions was presented. However, the crack initiation and propagation modes can be found from Ref. [31]. Table 9 shows the types of creep-fatigue crack initiation and propagation for different strengthening types of superalloys at temperature of 850 °C and 1.0% total strain. As the dwell time increases from 3 to 30 min, most cracks in DZ445 superalloy originate from the *trans*-granular mode and propagate along the grain boundary. For Haynes 230 and Alloy 617, the crack initiation mode gradually changes from transgranular to intergranular. In the case when dwell-time is 30 min, all the cracks originate in the intergranular mode. Then, they propagate in the transgranular or intergranular/transgranular mixed mode (Table 9 and Fig. 8). Generally speaking, the crack propagation rate of intergranular cracking is faster than that of transgranular cracking [55]. Based on the previous research, it would be reasonable to conclude that the crack initiation life of SC (single crystal) superalloys accounted for 90% of the total fatigue life [61]. The crack propagation mode shown in Table 9 corresponds to the fatigue life of DZ445 superalloy which is much higher than that of Haynes 230 and Alloy 617. The fatigue life of these two

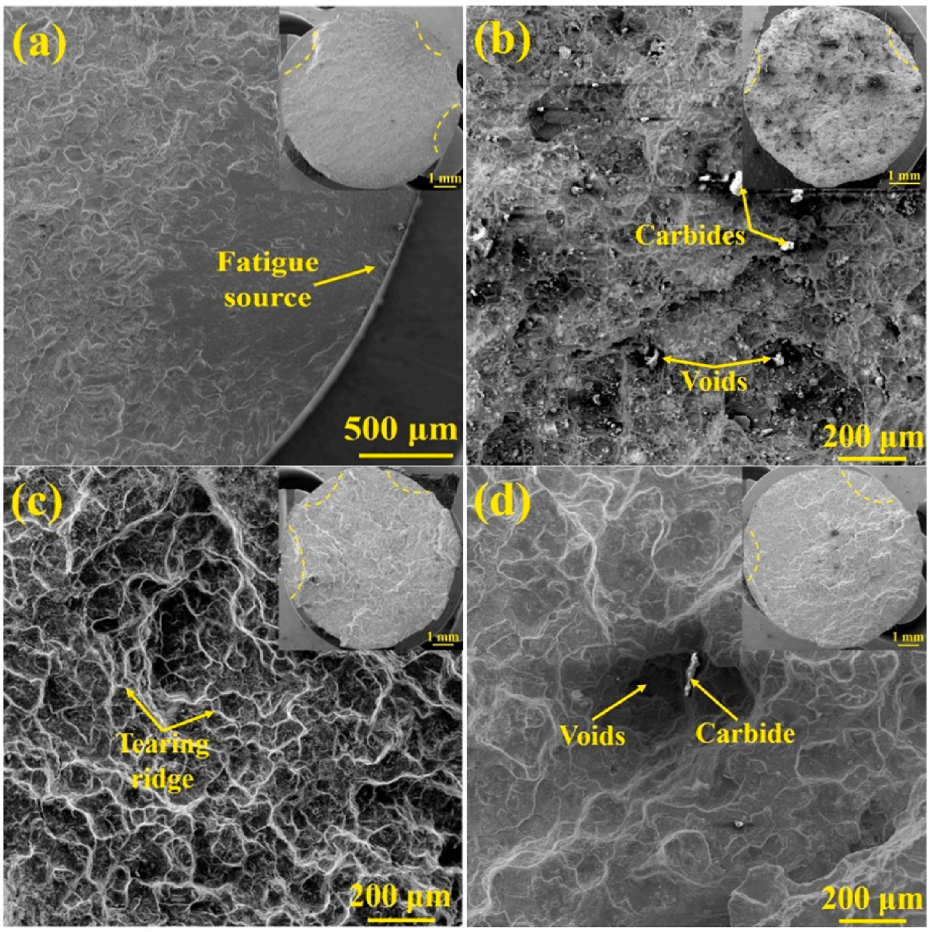

Fig. 6. Local enlarged view of creep-fatigue fracture of DZ445 superalloy under a total strain of 1.0% and temperature of 850 °C with dwell time (a) 0 min; (b) 3 min; (c) 10 min; (d) 30 min (The illustration in the upper right corner of the figure is the full view of the fracture; the area indicated by the yellow dotted line is the crack-initiation area). (For interpretation of the references to colour in this figure legend, the reader is referred to the Web version of this article.)

Table 9
Type of crack initiation and propagation for DZ445 superalloy, Alloy 617 [27], and Haynes 230 [27] at a total strain of 1.0% and 850 °C with different dwell time. (T = Transgranular and I = intergranular).

Parameters		1.0%, 0 min	1.0%, 3 min	1.0%, 10 min	1.0%, 30 min
DZ445	Initiation	T	T	T	T
	Propagation	T	T + I	I	I
Alloy 617	**Initiation**	T	I	I	I
	Propagation	T	I	I + T	I + T
Haynes 230	**Initiation**	T	T	T	I
	Propagation	T	T	T	T

solid-solution-strengthened superalloys continues to decrease with dwell time. In order to further show the influence of type of superalloy and dwell time on crack propagation path, the images of the fracture profile for these three superalloys are also shown as follow.

3.3.2. Crack damage

Fig. 7 shows the creep-fatigue profile crack diagram for DZ445 superalloy with different dwell time. As shown in Fig. 7 (a), narrow and long surface cracks perpendicular to the stress direction generally occur during pure low-cycle fatigue deformation. The low-cycle fatigue damage process is mainly controlled by time-independent surface cracks [56]. Together with the relative short time at high temperatures under the condition of pure fatigue, there are almost no internal voids or cracks. As the tensile dwell-time increases to 3 min [Fig. 7 (b)], the mean opening-angle and length of the profile cracks are increased and gradually decreases, respectively. When the dwell time increases to 10 and 30 min [Fig. 7 (c) and (d)], the opening-angle of the profile cracks increases, and the mean crack-length is further reduced, respectively. The statistical results of the mean length and opening-angle for these cracks and their standard deviations with different dwell time are shown in Table 10. In conditions of pure fatigue, narrow and elongated cracks were observed, while the blunt cracks are usually present after long dwell time (10 and 30 min) are applied. For example, in the conditions of pure-fatigue, the mean length and opening-angle of surface cracks are 112.65 μm and 4.24°, respectively. While they are 95.45 μm and 21.54° with 30 min dwell time, respectively.

The previous literature only shows the representative images of the solid-solution-strengthened superalloy Haynes 230 and Alloy 617 at temperature of 850 °C, 1.0% total strain after the creep-fatigue deformation [27]. Therefore, it is impractical to calculate the mean length and opening-angle of the creep-fatigue cracks of these two alloys here. Figs. 8 and 9 show the typical crack morphologies of Haynes 230 and Alloy 617 respectively. The intergranular cracks usually appear at 45° or perpendicular to the axial stress. The internal cracks are present around carbides [57]. With the application of the 3–30 min dwell time, the crack initiation and propagation are both in transgranular or transgranular/intergranular mixed modes. Many broken carbides and microcracks gradually grow to form the internal cavities. Previous investigations also show that there are high-density internal cracks with long dwell time [58]. There are more time for the voids to grow as the dwell time increases [59]. The crack length increases with the dwell time, resulting in a gradual increase in creep damage. Thus, the fatigue

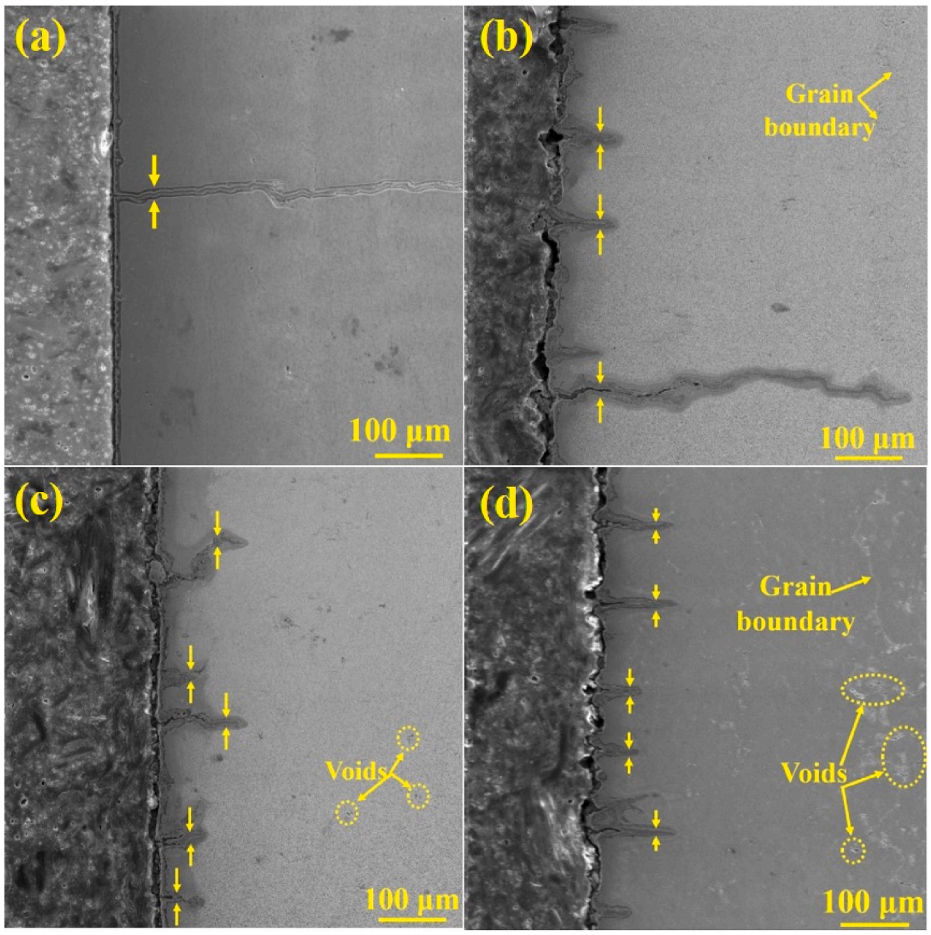

Fig. 7. Lateral crack morphology of DZ445 superalloy under a total strain of 1.0% and 850 °C with different dwell time (a) 0 min; (b) 3 min; (a) 10 min; (a) 30 min.

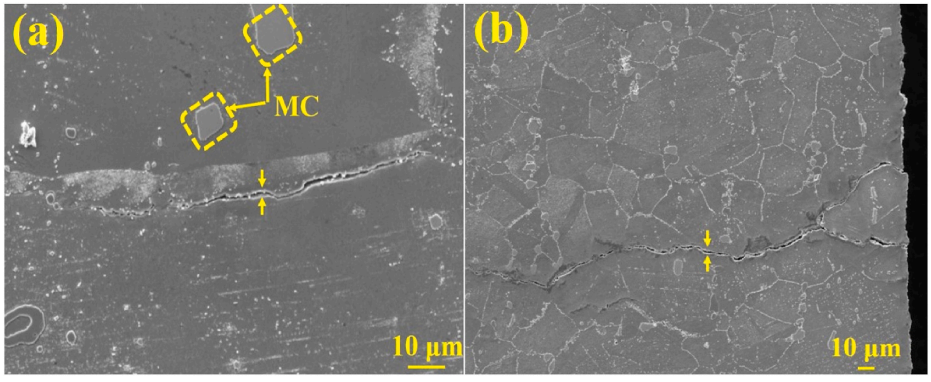

Fig. 8. Lateral crack morphology of Haynes 230 under a total strain of 1.0% and 850 °C with different dwell time (a) 3 min; (b) 30 min [27].

Table 10
Variation in mean length and opening angle of cracks for DZ445 superalloy at temperature of 850 °C with a total strain range of 1.0%. The D_T, $\overline{CL}$, $\overline{Angle}$, and σ represent the dwell time, mean crack length, mean crack opening-angle, and standard deviation, respectively.

Materials	D_T(min)	$\overline{CL}$ (μm)	σ (μm)	$\overline{Angle}$ (°)	σ (°)
DZ445	0	112.65	48.78	4.24	1.54
DZ445	3	98.45	59.91	11.45	8.74
DZ445	10	89.18	68.65	18.98	9.45
DZ445	30	95.45	55.54	21.54	8.65

life continues to decrease. Images from the literature also show that there are trigeminal-intergranular cracks and voids in Haynes 230 and Alloy 617 [27]. The intergranular damage in the form of creep voids caused by the dwell period not only provides additional crack initiation sites, but their growth/coalescing under tensile stress acts as a connection bridge to accelerate crack propagation. These factors contribute to the continue decrease of creep-fatigue life. The combined effect of stress and temperature can also cause the changes in the morphology of the γ′ phase for the precipitated-strengthened superalloy.

3.3.3. γ′ precipitate

Compared with the solid-solution-strengthened superalloys, the most

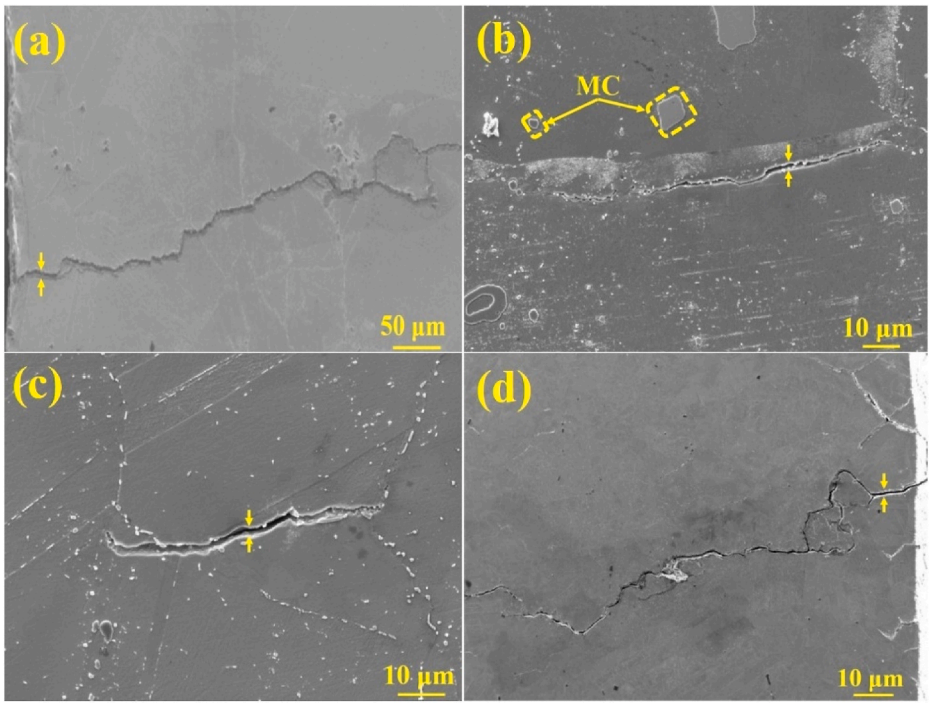

Fig. 9. Lateral crack morphology of Alloy 617 under total strain of 1.0% and temperature of 850 °C with different dwell time (a) 0 min; (b) 3 min; (a) 10 min; (a) 30 min [27].

important contribution to the outstanding high-temperature mechanical properties for the precipitation-strengthened superalloys could be attributed to the presence of cubic γ′ precipitates [60]. Fig. 10 shows the γ′ phase morphology for the DZ445 superalloy at a total strain of 1.0% and 850 °C. Compared with the appearance of original cubic γ′ phase in Fig. 1(b), the γ′ phases no longer maintain the regular cubic shape under the pure fatigue conditions [Fig. 10 (a)]. As the dwell time increases to 3 min [Fig. 10 (b)], the γ′ rafting begins to appear. But the rafting in this case is not complete. As the dwell time increases to 10 min [Fig. 10 (c) and (d)], the *N*-type rafting phenomenon with obvious twisting of γ′ could be observed. The γ′ rafting is more complete under the 30-min dwell time. The rafting is thought to be detrimental to creep properties [61], which reduces the creep-fatigue life of the superalloy. However, the appearance of dislocation networks under long dwell time delay the propagation of cracks [62] (it will be explained in detail in the next section). These two factors compete with each other and jointly affect the cyclic life.

The Cr-rich $M_{23}C_6$ and W-rich M_6C are the common precipitates in Haynes 230 and Alloy 617, respectively [25,27]. These precipitates on the grain boundary has been proven in other investigations to cause

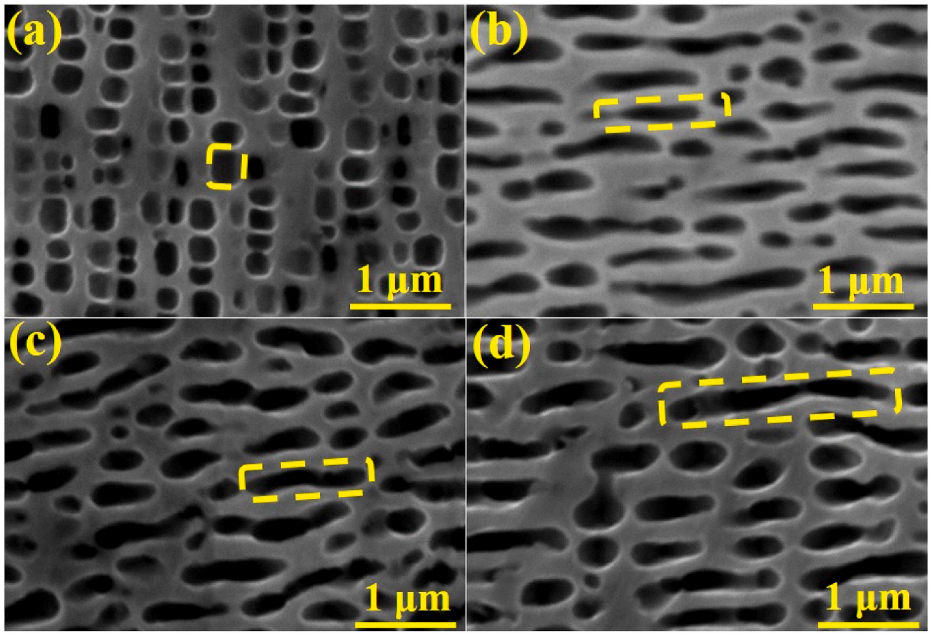

Fig. 10. γ′ precipitate morphology of DZ445 superalloy at a total strain of 1.0% and temperature of 850 °C (a) 0 min; (b) 3 min; (c) 10 min; (d) 30 min (The yellow dashed area is a the γ′ phase.). (For interpretation of the references to colour in this figure legend, the reader is referred to the Web version of this article.)

premature fracture failure and reduce the cyclic life [27]. For the creep-fatigue behavior of 316 stainless steel at 593 °C, the fatigue life with the dwell time of 1440 min is higher than that when the dwell time is 600 min at the total strain range is 2.0% [63]. This phenomenon may be caused by the aging of the material with long dwell time. The aging process causes the coarsening of the precipitate in the matrix, restricting the sliding of the grain boundary. Thus, the stress concentration at the precipitate/matrix interface is reduced, which delays the interconnection of the voids and increases the fatigue life [63]. The fracture characteristics of these superalloys was shown qualitatively and semi-quantitatively above. The evolution of fracture behavior is essentially controlled by the dislocations structure.

3.3.4. Dislocation structure

Fig. 11 shows the dislocation morphology of DZ445 superalloy at a total strain of 1.0% and 850 °C with different dwell time. In the case of

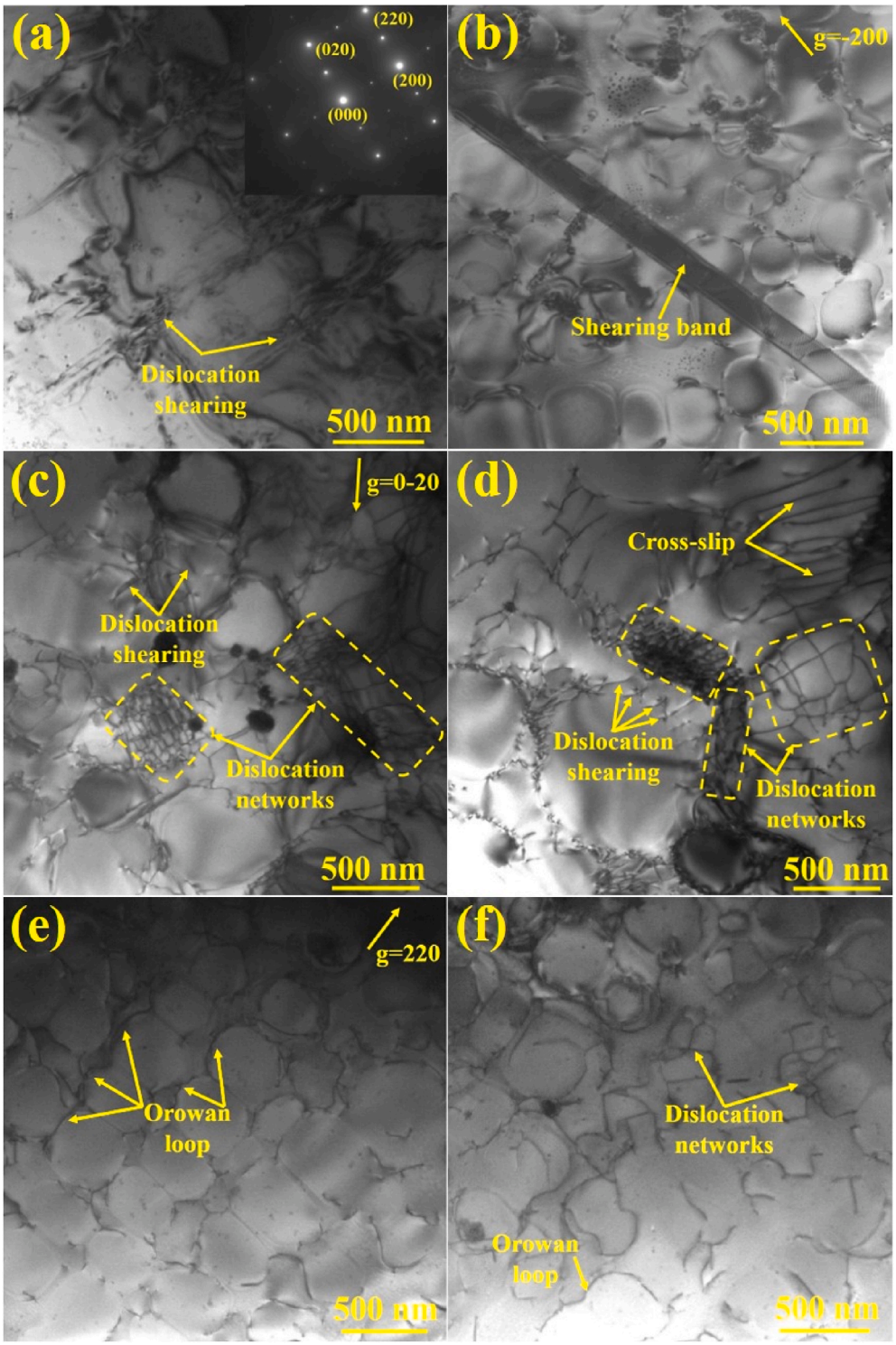

Fig. 11. Dislocation configuration of DZ445 superalloy at a total strain of 1.0% and temperature of 850 °C with different dwell time (a), (b) 0 min; (c), (d) 3 min; (e), (f) 10 min (The g is the operating vector in two beam conditions. The inset of Fig. 1 (a) showing the diffraction spot at Beam//[001]).

low-cycle-fatigue [Fig. 11 (a) and (b)], the dislocations in the γ matrix encounter the γ′ precipitates and then cut into the phases. Occasionally, long-strip dislocations through the γ and γ′ phases can be found to achieve the desired plastic deformation. As the dwell time increases to 3 min [Fig. 11(c) and (d)], some dislocations cut into the γ′ precipitate. Other dislocations are rearranged and more dislocations are arranged at the γ/γ′ interface. A small amount of dislocation networks are also formed. The interaction of creep and fatigue greatly reduces the cyclic life. In addition, after applying the dwell time, the sample is exposed at high temperature for a long time. Due to the severe thermal activation and the higher relative strength of the γ/γ′ phase, the dislocations become more active in the cross-slip and climb modes. This leads to the rapid development of the dislocation network at the γ/γ′ interface, resulting in the cyclic softening [64]. When the dwell time is further increased to 10 min [Fig. 11(e) and (f)], more dislocations are arranged at the γ/γ′ interface. Few dislocations can be cut into γ′ when they meet. The dislocation network on the γ/γ′ interface mostly bypass the γ′ precipitate in the form of Orowan loop. The dislocations bow out to bypass the γ′ phase by critical stress (τ),

$$\tau = \frac{Gb}{2r} \tag{3}$$

where G, b, and r are the shear modulus, Burgers vector, and the width of the γ channel, respectively. With the dissolution of γ′ corners and the coarsening of γ′ phase after the application of dwell time, the width of γ channel increases and then the Orowan critical shear stress decreases. In order to encourage the development of uniform dislocation slip, it takes more time for the dislocation to cross the γ′ phase with large size. Occasionally, few mobile superdislocations cut into the γ′ precipitate. The process of the dissolution of these γ′ precipitates and the recovery of dislocations is the cause of the cyclic softening. The entanglement of dislocations will cause the cyclic hardening. When the above two dislocation structures reach a dynamic equilibrium, the cyclic steady is formed as shown in Fig. 3(a).

As shown in Fig. 12, as the dwell time is increased to 30 min, the dislocation density is greatly increased. The dislocation networks, dislocation loops, and some dislocation entanglements are present at the γ/γ′ interface. The contrast of bright and dark field images in Fig. 12 (c) and (d) can show the dislocation structure more clearly. As reported by Décamps [65] et al., the interfacial dislocation network may prevent other dislocations from cutting into the γ′ precipitate, causing a slower reduction of cyclic life for DZ445 superalloy with 30 min dwell time.

According to the typical creep-fatigue dislocations of Alloy 617 recorded in the literatures [25,66] at temperature of 850 °C, it is found that there is no obvious dislocation subgrain structure during low-cycle fatigue deformation. There are large number of mobile dislocations [Fig. 13(a)]. Obvious dislocation subgrain structure appears in the process of creep-fatigue deformation. These substructures were originally formed by entangled dislocations in the dislocation wall. Further cyclic deformation promotes the climbing, the rearrangement, and the interaction of dislocations from subgrains. They gradually evolve into the dislocations network, forming subgrain boundaries [Fig. 13 (b and c)]. At 850 °C, there are many mobile dislocations distributed in the subgrain. The inelastic strain rate ($\dot{\varepsilon}_{in}$) is proportional to mobile dislocation density [67],

$$\dot{\varepsilon}_{in} = \rho_m b v \tag{4}$$

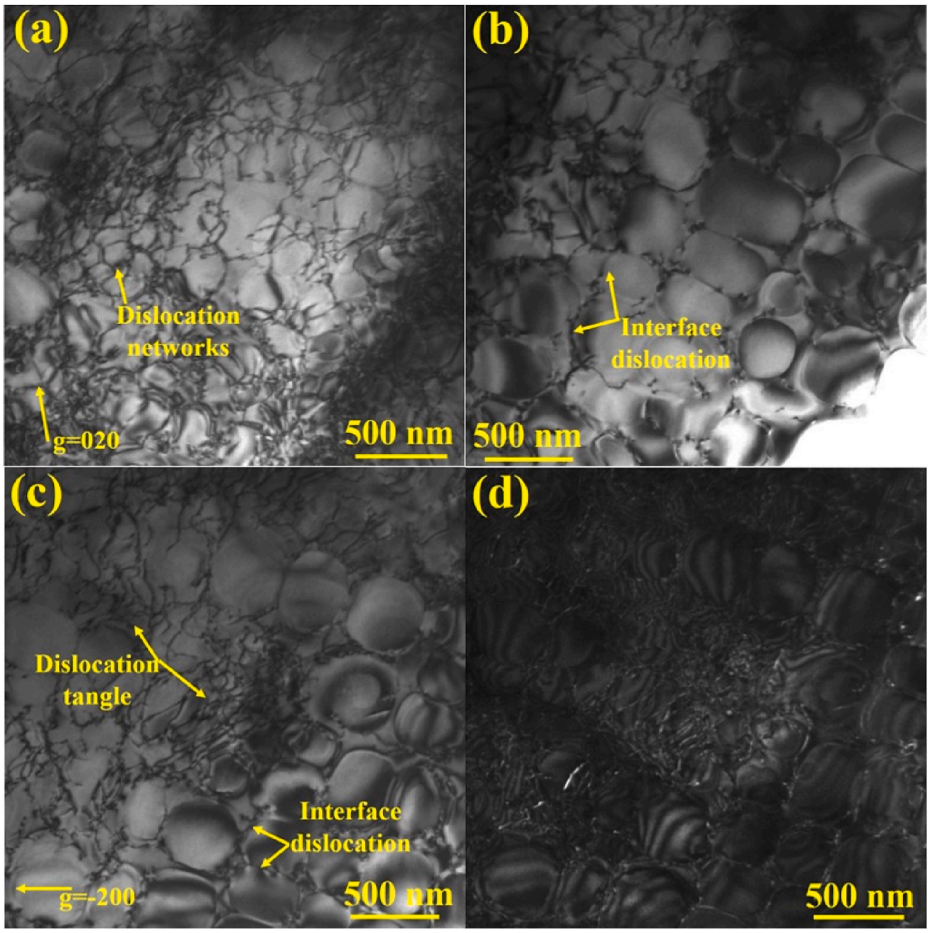

Fig. 12. Dislocation configuration of DZ445 superalloy at a total strain of 1.0% and temperature of 850 °C with dwell time of (a–c) 30 min in bright-field-image mode; (d) dark-field-image mode. (The g is the operating vector in two beam conditions).

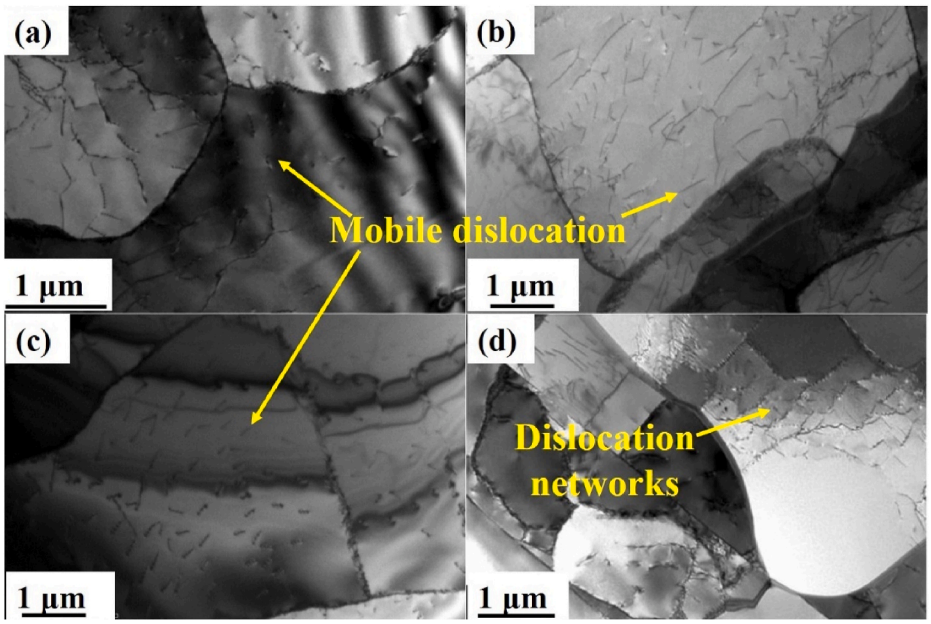

Fig. 13. Dislocation configuration of Alloy 617 at a total strain of 0.3% and temperature of 850 °C with dwell time of (a) 0 min, (b) 3 min, (c) 10 min [25]; (d) at a total strain of 0.3% and 950 °C with dwell time of 10 min [66].

where ρ_m, b, and v are the density of dislocations, Burgers vector, and dislocation migration rate, respectively.

The mobile dislocation density is still high after the dwell time is applied at temperature of 850 °C. It will increase the inelastic deformation rate and reduce the fatigue life. While in the creep-fatigue deformation at temperature of 950 °C, where the saturation effect of N_f occurs in the same strain range, the creep-fatigue fracture substructure is still composed of sub-grains, there are no mobile dislocations in the matrix [Fig. 13(d)]. An ordered arrangement of dislocations or network boundaries appears. Boundary dislocations contain a large number of kinks, indicating that there are quite a lot of dislocation interactions before or during their arrangement into an ordered networks [66]. Compared to the temperature of 850 °C, the density of mobile dislocations within creep-fatigue samples deformed at temperature of 950 °C is much lower corresponding to the fact that the fatigue life saturation is more likely to occur at temperature of 950 °C than that at 850 °C. The dislocation movement mechanism of Haynes 230 is not explained in the literature. Thus, we only select the creep-fatigue dislocation structure of Alloy 617 for detailed analysis. We have revealed the occurrence conditions of the creep-fatigue N_f saturation effect for different types of superalloys from the perspective of dislocations.

4. Discussion

4.1. Intrinsic relationship between mechanical response and damage mechanism

Through the above analysis, the appearance of N_f saturation effect, mechanical response, and damage parameters for the three different strength superalloys are summarized in detail in Table 11. It can be concluded that in the creep-fatigue deformation, the N_f saturation phenomenon is prone to occur when the stress is stable, the number of mobile superdislocations is few, or when the mobile superdislocations reach dynamic equilibrium with the dislocation network after the dwell time is applied. To the contrary, the cyclic life tends to decrease with dwell time continuously.

Table 11
Summary of creep-fatigue mechanical response and damage characteristics for DZ445 superalloy (a); Haynes 230 [27], and Alloy 617 [27] at a total strain of 1.0% and 850 °C.

Materials	D_T (min)	Occurrence conditions of N_f saturation	Maximum stress	Crack	Dislocation
DZ445	Short	Easy	Steady	Narrow & long	Cutting into γ′
	Long			Blunt & short	Orowan bypass + dislocation networks
Haynes 230	Short	Difficulty	Continuous decline	Narrow & long	/
	Long			Blunt & long	/
Alloy 617	Short	Difficulty	Continuous decline	Narrow & short	Cells + mobile dislocation
	Long			Blunt & long	Subgrains + mobile dislocation

4.2. Evaluation of fracture time

In the traditional test for determining the material mechanical, properties, we take the fracture time as an index for estimating the creep property, and the number of cycles as a parameter for estimating the fatigue performance, respectively [68]. According to the number of cycles, the creep-fatigue belongs to the category of low-cycle-fatigue deformation. The cyclic life is usually used as an index to evaluate the creep-fatigue performance. Fig. 14 shows the relationship between tensile-dwell time (t_d) and fracture time (t_f) of these three superalloys at the temperature of 850 °C and a total strain range of 1.0%, The expression of t_f is [21]:

$$t_f = \frac{N_f}{f} + N_f \cdot t_d \tag{6}$$

where f is the frequency of pure low-cycle fatigue loading, which can be calculated by the following formula:

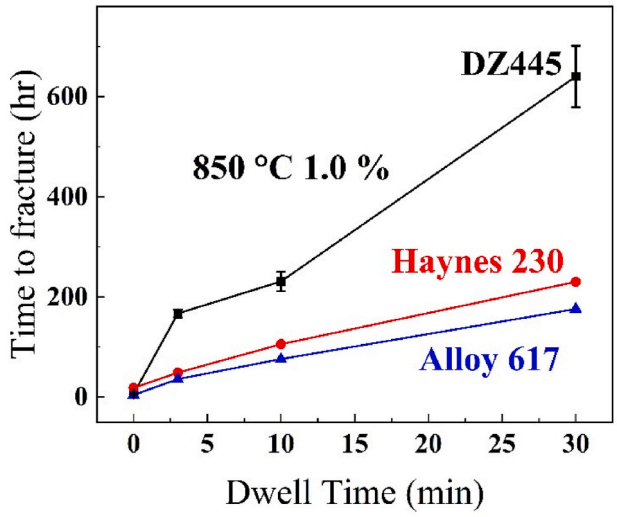

Fig. 14. Relationship between tensile dwell-time (t_d) and fracture time (t_f) for DZ445 superalloy (a); Haynes 230 [27], and Alloy 617 [27] with different dwell time at a total strain of 1.0% and 850 °C.

$$f = \frac{\dot{\varepsilon}}{2\Delta\varepsilon_t} \tag{7}$$

where $\dot{\varepsilon}$ is the strain rate in the cyclic loading and unloading stages, and the $\Delta\varepsilon_t$ is the total strain range. In this investigation, the total strain range $\Delta\varepsilon_t$ is 1.0%, and the strain rates ($\dot{\varepsilon}$) of DZ445, Haynes 230, and Alloy 617 are $5 \times 10^{-3}s^{-1}$, $2.5 \times 10^{-4}s^{-1}$, and $2.5 \times 10^{-4}s^{-1}$, respectively. The length of the gauge length is 25 μm, 6 μm, and 12 μm, respectively. Therefore, the fracture time could also be obtained,

$$t_f = N_f\left(\frac{2\Delta\varepsilon}{\dot{\varepsilon}} + t_d\right) \tag{8}$$

It can be seen from Fig. 14 that the fracture time increases with increasing dwell time for these three superalloys. This trend seems to be opposite to the creep-fatigue cyclic life in Fig. 2 with dwell time. In fact, this trends are reasonable because compared with the definition of cyclic life, the dwell time factor is added to the expression of fracture time. This factor has an effect on fracture time (t_f), which is greater than the decrease of cycle life (N_f) [69]. Therefore, the introduction of dwell time will cause a decrease in the creep-fatigue cyclic life and an increase in the fractue time. Nagae once proposed the relationship between fracture time and fracture energy in the creep-fatigue deformaion [70]. It has been proved that it has a good accuracy in extrapolating service life. Therefore, when evaluating the creep-fatigue service performance, we should not only focus on the service cycles in conjunction with Fig. 2. For long-term dwell load, the total service rupture time shown in Fig. 14 is also an important parameter when the cyclic life is saturated.

4.3. The meaning of saturation

Although previous researchers have disovered the N_f saturation effect under long dwell time in creep-fatigue deformation, it has not been extensively investigated. Regarding the relationship between dwell time and fatigue life with different strengths of superalloy in Fig. 2, we discovered and elaborated on that "occurrence condition of the N_f saturation" and the corresponding mechanism. The creep-fatigue life saturation effect is an important phenomenon that can have a substantial impact on experimental research and even actual service, because it can reduce the test time when the cyclic life is saturated. In other words, once the saturation limit of a given material is reached, the use of longer dwell time tests can be eliminated or at least significantly reduced. In the creep-fatigue test of 9Cr-0.5 Mo-1.8 WV-Nb thermal resistance steel, without performing the creep-fatigue test for 60 min of compression dwell time is not only because the long dwell load creep-fatigue test is cost. But also the saturation life of the creep-fatigue test is achieved within 10 min of compression dwell time [71]. Due to the consideration of economic benefits, the actual service behavior is usually extrapolated from short-term experiments. Another important significance of the saturation effect is that it can better predict the creep-fatigue rupture time when the creep-fatigue cyclic life tends to be saturated. When the loading conditions are constant, the relationship between the fracture time of different materials and the tensile dwell time tends to be linear. Thus, the fracture time under long dwell time can be extrapolated. It provides the theoretical guidance for the creep-fatigue safety design of superalloys.

5. Conclusions

In this study, the strain-controlled creep-fatigue experiments were performed on the precipitation-strengthened superalloy DZ445 at 850 °C and 1.0% total strain range. Combined with the data of Haynes 230 and Alloy 617 under the same loading conditions, the occurrence conditions of N_f saturation effect for three superalloys is systematically analyzed from mechanical response, crack damage, and deformation mechanism. Based on the above results and analysis, the following conclusions can be drawn:

(1) As the dwell time increases from 0 to 30 min, the decline of creep-fatigue life for DZ445 superalloy decreases gradually (i.e. the generalized N_f saturation effect); while the fatigue life of Alloy 617 and Haynes 230 continues to decrease. The fracture life of the three superalloys increases with dwell time continuously.
(2) When no dwell time is applied to the DZ445 superalloy, the maximum stress is almost flat during the entire deformation process. After the dwell time is applied, the maximum tensile stress drops rapidly and then reaches an approximate steady state. However, the maximum tensile stress of Haynes 230 and Alloy 617, which are mainly strengthened by solid solution, showed a continuous decrease in the entire deformation.
(3) Regardless of the total dwell time, the relaxation stress curve of DZ445 superalloy shows the following three stages: rapid softening, transition, and final stable stage. However, the stresses in the dwell period of solid-solution-strengthened Alloy 617 and Haynes 230 continue to relax.
(4) As the dwell time increases, the lateral cracks of DZ445 superalloy change from slender-to blunt-mode. The crack damage of Haynes 230 and Alloy 617 continues to increase with dwell time.
(5) For the precipitation-strengthened DZ445 superalloy, as the dwell time is increased to 10 and 30 min, few dislocations cut into the γ′ precipitate. Orowan bypass, γ/γ′ interface dislocation networks, and some dislocation entanglements are dominated. The Alloy 617, which is mainly strengthened by solid-solution, is dominated by dislocation cells after creep-fatigue deformation. The density of mobile dislocation is relatively high.

CRediT authorship contribution statement

Biao Ding: Methodology, carried out the main experiments, Formal analysis, Writing – original draft, discussed the results and commented on the manuscript. **Weili Ren:** Methodology, Formal analysis, Writing – original draft, discussed the results and commented on the manuscript. **Yunbo Zhong:** processed the alloy samples, Formal analysis, Writing – original draft, discussed the results and commented on the manuscript. **Xiaotan Yuan:** discussed the results and commented on the manuscript. **Tianxiang Zheng:** discussed the results and commented on the manuscript. **Zhe Shen:** Formal analysis, Writing – original draft, discussed the results and commented on the manuscript. **Yifeng Guo:** processed the alloy samples, discussed the results and commented on the manuscript.

Qiang Li: discussed the results and commented on the manuscript. **Chunmei Liu:** discussed the results and commented on the manuscript. **Jianchao Peng:** conducted the TEM characterization, discussed the results and commented on the manuscript. **Josip Brnic:** Formal analysis, Writing – original draft, discussed the results and commented on the manuscript. **Yanfei Gao:** Formal analysis, Writing – original draft, discussed the results and commented on the manuscript. **Peter K. Liaw:** Formal analysis, Writing – original draft, discussed the results and commented on the manuscript.

Declaration of competing interest

The authors declare that they have no known competing financial interests or personal relationships that could have appeared to influence the work reported in this manuscript.

Acknowledgments

W.L.R. is grateful for financial supports from the National Science Foundation of China (NSFC) (Grant number 51871142), the Independent Research and Development Project of State Key Laboratory of Advanced Special Steel, Shanghai Key Laboratory of Advanced Ferrometallurgy, Shanghai University (SKLASS 2020-Z04) and the Science and Technology Commission of Shanghai Municipality (No. 19DZ2270200). B.D. is grateful for the financial support from the fellowship of China Postdoctoral Science Foundation (2021M692020). Y.B.Z. is grateful for the financial support from the National Key Research and Development Program of China (2018YFF0109404, 2016YFB0300401, and 2016YFB0301401), the National Natural Science Foundation of China (U1732276 and U1860202). P. K. L. very much appreciates the supports from the National Science Foundation (DMR-1611180 and 1809640) with the program directors, Drs. Judith Yang, Gary Shiflet, and Diana Farkas.

References

[1] S. Suresh, Fatigue of Materials, Cambridge Univ Press, Cambridge, UK, 1998.
[2] R.C. Reed, The Superalloys: Fundamentals and Applications, Cambridge university press, 2008.
[3] F. Tahir, Y. Liu, A new experimental testing method for investigation of creep-dominant creep-fatigue interaction in Alloy 617 at 950 °C, Int. J. Pres. Ves. Pip. 154 (2017) 75–82.
[4] D. Barbera, H. Chen, Y. Liu, On creep fatigue interaction of components at elevated temperature, J. Pressure Vessel Technol. 138 (4) (2016).
[5] T.M. Pollock, Alloy design for aircraft engines, Nat. Mater. 15 (8) (2016) 809–815.
[6] R.Z. Wang, J. Wang, J.G. Gong, et al., Creep-fatigue behaviors and life assessments in two nickel-based superalloys, J. Pressure Vessel Technol. 140 (3) (2018).
[7] R.Z. Wang, X.C. Zhang, S.T. Tu, et al., The effects of inhomogeneous microstructure and loading waveform on creep-fatigue behaviour in a forged and precipitation hardened nickel-based superalloy, Int. J. Fatig. 97 (2017) 190–201.
[8] R.Z. Wang, X.C. Zhang, J.G. Gong, et al., Creep-fatigue life prediction and interaction diagram in nickel-based GH4169 superalloy at 650 °C based on cycle-by-cycle concept, Int. J. Fatig. 97 (2017) 114–123.
[9] F. Tahir, S. Dahire, Y. Liu, Image-based creep-fatigue damage mechanism investigation of Alloy 617 at 950 °C, Mater. Sci. Eng., A 679 (2017) 391–400.
[10] Y.L. Lu, P.K. Liaw, Y. Sun, et al., Hold-time effect on the elevated-temperature crack growth behavior of solid-solution-strengthened superalloys, Acta Mater. 55 (3) (2007) 767–775.
[11] Y.L. Lu, L.J. Chen, G.Y. Wang, et al., Hold time effects on low cycle fatigue behavior of HAYNES 230® superalloy at high temperatures, Mater. Sci. Eng., A 409 (1–2) (2005) 282–291.
[12] G. Chen, Y. Zhang, D.K. Xu, et al., Low cycle fatigue and creep-fatigue interaction behavior of nickel-base superalloy GH4169 at elevated temperature of 650 °C, Mater. Sci. Eng., A 655 (2016) 175–182.
[13] L.J. Carroll, C. Cabet, M.C. Carroll, et al., The development of microstructural damage during high temperature creep–fatigue of a nickel alloy, Int. J. Fatig. 47 (2013) 115–125.
[14] D. Shi, J. Liu, X. Yang, et al., Experimental investigation on low cycle fatigue and creep–fatigue interaction of DZ125 in different dwell time at elevated temperatures, Mater. Sci. Eng., A 528 (1) (2010) 233–238.
[15] W. Zhang, X. Wang, H. Chen, et al., Evaluation of the effect of various prior creep-fatigue interaction damages on subsequent tensile and creep properties of 9% Cr steel, Int. J. Fatig. 125 (2019) 440–453.
[16] A. Chauhan, L. Straßberger, U. Führer, et al., Creep-fatigue interaction in a bimodal 12Cr-ODS steel, Int. J. Fatig. 102 (2017) 92–111.
[17] S. Zamrik, Symposium on Design for Elevated Temperature Environment, American Society of Mechanical Engineers, 1971.
[18] X. Zhang, S.T. Tu, F. Xuan, Creep–fatigue endurance of 304 stainless steels, Theor. Appl. Fract. Mech. 71 (2014) 51–66.
[19] J. Wareing, Creep-fatigue behaviour of four casts of type 316 stainless steel, Fatig. Fract. Eng. Mater. Struct. 4 (2) (1981) 131–145.
[20] J.K. Wright, L.J. Carroll, C. Cabet, et al., Characterization of elevated temperature properties of heat exchanger and steam generator alloys, Nucl. Eng. Des. 251 (2012) 252–260.
[21] H.P. Meurer, G.K.H. Gnirss, W. Mergler, et al., Investigations on the fatigue behavior of high-temperature alloys for high-temperature gas-cooled reactor components, Nucl. Technol. 66 (2) (1984) 315–323.
[22] R.K. Rai, J.K. Sahu, S.K. Das, et al., Creep-fatigue deformation micromechanisms of a directionally solidified nickel-base superalloy at 850 °C, Fatig. Fract. Eng. Mater. Struct. 43 (1) (2020) 51–62.
[23] L.R. Zeng, L.M. Lei, X.M. Luo, et al., Toward an understanding of dwell fatigue damage mechanism of bimodal Ti-6Al-4V alloys, J. Mater. Sci. Technol. 108 (2022) 244–255.
[24] C.Q. Sun, Y.Q. Li, K.L. Xu, et al., Effects of intermittent loading time and stress ratio on dwell fatigue behavior of titanium alloy Ti-6Al-4V ELI used in deep-sea submersibles, J. Mater. Sci. Technol. 77 (2021) 223–236.
[25] L. Carroll, Progress Report on Long Hold Time Creep Fatigue of Alloy 617 at 850° C, Idaho National Lab, INL, Idaho Falls, ID (United States), 2015.
[26] L. Carroll, C. Cabet, M. Carroll, Wright, The development of microstructural damage during high temperature creep–fatigue of a nickel alloy, Int. J. Fatig. 47 (2013) 115–125.
[27] X. Chen, High Temperature Creep-Fatigue Behavior of Alloy 617 and Alloy 230, University of Illinois at Urbana-Champaign, 2012.
[28] C. Xu, L.Z. Zhou, J.T. Guo, et al., Effect of withdrawal rate on microstructures and mechanical properties of directionally solidified superalloy DZ445, Chin. J. Nonferrous Metals 21 (4) (2011) 757.
[29] X. Xiao, H. Xu, X. Qin, et al., Thermal fatigue behavior of three cast nickel-base superalloys, Acta Metall. Sin. 28 (2011) 1129–1134.
[30] B. Ding, W. Ren, K. Deng, et al., An abnormal increase of fatigue life with dwell time during creep-fatigue deformation for directionally solidified Ni-based superalloy DZ445, High Temp. Mater. Process. 37 (3) (2018) 277–284.
[31] S.Y. Lee, Y.L. Lu, P.K. Liaw, et al., Tensile-hold low-cycle-fatigue properties of solid-solution-strengthened superalloys at elevated temperatures, Mater. Sci. Eng., A 504 (1–2) (2009) 64–72.
[32] K. Hrutkay, D. Kaoumi, Tensile deformation behavior of a nickel based superalloy at different temperatures, Mater. Sci. Eng., A 599 (2014) 196–203.
[33] D. Kaoumi, K. Hrutkay, Tensile deformation behavior and microstructure evolution of Ni-based superalloy 617, J. Nucl. Mater. 454 (1–3) (2014) 265–273.
[34] X. Chen, Z. Yang, M.A. Sokolov, et al., Low cycle fatigue and creep-fatigue behavior of Ni-based alloy 230 at 850 °C, Mater. Sci. Eng., A 563 (2013) 152–162.
[35] K. Barat, S. Sivaprasad, S. Kar, et al., Creep fatigue interaction under different test variables: mechanics and mechanisms, J. Test. Eval. 46 (6) (2018) 2521–2539.
[36] E.A. Estrada Rodas, S. Gorgannejad, R.W. Neu, Creep-fatigue behaviour of single-crystal Ni-base superalloy CMSX-8, Fatig. Fract. Eng. Mater. Struct. 42 (9) (2019) 2155–2171.
[37] K. Kobayashi, M. Hayakawa, M. Kimura, Creep-fatigue interaction properties of nickel-based superalloy 617, Acta Metall. Sin. 24 (2) (2011) 125–131.
[38] U. Führer, J. Aktaa, Modeling the cyclic softening and lifetime of ferritic-martensitic steels under creep-fatigue loading, Int. J. Mech. Sci. 136 (2018) 460–474.
[39] L. Zhao, L. Xu, Y. Han, et al., Modelling creep-fatigue behaviours using a modified combined kinematic and isotropic hardening model considering the damage accumulation, Int. J. Mech. Sci. 161 (2019), 105016.
[40] I. Šulák, K. Obrtlík, Effect of tensile dwell on high-temperature low-cycle fatigue and fracture behaviour of cast superalloy MAR-M247, Eng. Fract. Mech. 185 (2017) 92–100.
[41] Q. Yue, L. Liu, W. Yang, et al., Stress dependence of the creep behaviors and mechanisms of a third-generation Ni-based single crystal superalloy, J. Mater. Sci. Technol. 35 (5) (2019) 752–763.
[42] J. Mao, X. Li, D. Wang, et al., Experimental study on creep-fatigue behaviors of Chinese P92 steel with consideration of several important factors, Int. J. Fatig. 142 (2021), 105900.
[43] G.R. Halford, The energy required for fatigue(Plastic strain hystersis energy required for fatigue in ferrous and nonferrous metals), J. Mater. 1 (1966) 3–18.
[44] H. Xu, Study on Fatigue Properties of Directionally Solidified Nickel-Based Superalloy DZ445, Shenyang University of Technology, 2012, pp. 32–34.
[45] Y. Wang, J. Dong, M. Zhang, et al., Stress relaxation behavior and mechanism of AEREX350 and Waspaloy superalloys, Mater. Sci. Eng., A 678 (2016) 10–22.
[46] S. Rahimi, M. King, C. Dumont, Stress relaxation behaviour in IN718 nickel based superalloy during ageing heat treatments, Mater. Sci. Eng., A 708 (2017) 563–573.
[47] V. Agarwal, R. Wright, T. Roney, Prediction of the Creep-Fatigue Lifetime of Alloy 617: an Application of Non-destructive Evaluation and Information Integration, Idaho National Laboratory (INL), 2014.
[48] D.B. Bober, J. Lind, R.P. Mulay, et al., The formation and characterization of large twin related domains, Acta Mater. 129 (2017) 500–509.
[49] Y. Takahashi, B. Dogan, D. Gandy, Systematic evaluation of creep-fatigue life prediction methods for various alloys, J. Pressure Vessel Technol. 135 (6) (2013).
[50] L. Cui, J. Yu, J. Liu, et al., Cyclic stress responses of a newly developed nickel-base superalloy at elevated temperatures, J. Alloys Compd. 773 (2019) 250–263.

[51] L. Cui, J. Liu, R.L. Peng, et al., Low cycle fatigue behavior and microstructural evolution of nickel-based superalloy M951G at elevated temperatures, Mater. Char. 163 (2020), 110241.
[52] Y. Zhong, X. Liu, K.C. Lan, et al., On the biaxial thermal creep-fatigue behavior of Ni-base Alloy 617 at 950 °C, Int. J. Fatig. 139 (2020), 105787.
[53] Z. Zhao, X. Chen, Effect of cyclic softening and stress relaxation on fatigue behavior of 2.25 Cr1Mo0. 25V steel under strain-controlled fatigue-creep interaction at 728 K, Int. J. Fatig. 140 (2020), 105848.
[54] P. Duan, P. Zhang, J. Li, et al., Intermediate temperature brittleness in a directionally solidified nickel-based superalloy M4706, Mater. Sci. Eng., A 759 (2019) 530–536.
[55] M. Gell, G.R. Leverant, Mechanisms of High-Temperature fatigue//Fatigue at Elevated Temperatures, ASTM International, 1973.
[56] F.D. León-Cázares, R. Schlütter, T. Jackson, et al., A multiscale study on the morphology and evolution of slip bands in a nickel-based superalloy during low cycle fatigue, Acta Mater. 182 (2020) 47–59.
[57] T. Lillo, J. Cole, M. Frary, et al., Influence of grain boundary character on creep void formation in alloy 617, Metall. Mater. Trans. 40 (12) (2009) 2803.
[58] S. Goyal, K. Mariappan, V. Shankar, et al., Studies on creep-fatigue interaction behaviour of Alloy 617M, Mater. Sci. Eng., A 730 (2018) 16–23.
[59] L. Cui, H. Su, J. Yu, et al., The creep deformation and fracture behaviors of nickel-base superalloy M951G at 900 °C, Mater. Sci. Eng., A 707 (2017) 383–391.
[60] J.T. Guo, Superalloy materials (Volume II): superalloy materials and engineering applications, 48, 2010, pp. 151–180.
[61] Y.N. Fan, H.J. Shi, W.H. Qiu, Constitutive modeling of creep behavior in single crystal superalloys: effects of rafting at high temperatures, Mater. Sci. Eng., A 644 (2015) 225–233.
[62] W. Xia, X. Zhao, Q. Yue, et al., Formative and controlled mechanisms of nano-sized γ′ precipitates with local phase-transition within dislocation networks of nickel-based single crystal superalloys, Acta Mater. 206 (2021), 116653.
[63] X.L. Yan, X.C. Zhang, S.T. Tu, et al., Review of creep–fatigue endurance and life prediction of 316 stainless steels, Int. J. Pres. Ves. Pip. 126 (2015) 17–28.
[64] M.R. Daymond, M. Preuss, B. Clausen, Evidence of variation in slip mode in a polycrystalline nickel-base superalloy with change in temperature from neutron diffraction strain measurements, Acta Mater. 55 (9) (2007) 3089–3102.
[65] B. Décamps, V. Brien, A.J. Morton, Deformation microstructures after low-cycle fatigue at 950 C in Ni-based superalloys: the effect of test conditions, Scripta Metall. Mater. 31 (7) (1994) 793–798.
[66] M.C. Carroll, L.J. Carroll, Developing dislocation subgrain structures and cyclic softening during high-temperature creep–fatigue of a nickel alloy, Metall. Mater. Trans. 44 (8) (2013) 3592–3607.
[67] Y. Tang, M. Huang, J. Xiong, et al., Evolution of superdislocation structures during tertiary creep of a nickel-based single-crystal superalloy at high temperature and low stress, Acta Mater. 126 (2017) 336–345.
[68] C. Pei, D. Shi, H. Yuan, et al., Assessment of mechanical properties and fatigue performance of a selective laser melted nickel-base superalloy Inconel 718, Mater. Sci. Eng., A 759 (2019) 278–287.
[69] J.B. Conway, R.H. Stentz, J.T. Berling, Fatigue, Tensile, and Relaxation Behavior of Stainless Steels, Mar-Test, Inc., Cincinnati, Ohio (USA), 1975.
[70] Y. Nagae, Evaluation of creep–fatigue life based on fracture energy for modified 9Cr–1Mo steel, Mater. Sci. Eng., A 560 (2013) 752–758.
[71] X. Wang, W. Zhang, J. Gong, et al., Low cycle fatigue and creep fatigue interaction behavior of 9Cr-0.5 Mo-1.8 WV-Nb heat-resistant steel at high temperature, J. Nucl. Mater. 505 (2018) 73–84.